Int J Appl Earth Obs Geoinformation 91 (2020) 102162

Contents lists available at ScienceDirect

Int J Appl Earth Obs Geoinformation

journal homepage: www.elsevier.com/locate/jag

Integration of remote sensing, gravity and geochemical data for exploration of Cu-mineralization in Alwar basin, Rajasthan, India

Shovan Lal Chattoraj[a,*], Gokul Prasad[a], Richa U. Sharma[a], P.K. Champati ray[a], Freek D. van der Meer[b], Arindam Guha[c], Amin Beiranvand Pour[d]

[a] Indian Institute of Remote Sensing (ISRO), 4-Kalidas Road, Dehradun, India
[b] University of Twente, Faculty of Geo-Information Science and Earth Observation (ITC), Enschede, the Netherlands
[c] National Remote Sensing Centre, Balanagar, Hyderabad, India
[d] Institute of Oceanography and Environment (INOS), University Malaysia Terengganu (UMT), Kuala Nerus 21030, Terengganu, Malaysia

ARTICLE INFO

Keywords:
Mineral exploration
ASTER
SAM
Malachite
Favorability index

ABSTRACT

In spite of the dominance of traditional mineral exploration methods that demand physical characterization of rocks and intense field work, remote sensing technologies have also evolved in the recent past to facilitate mineral exploration. In the present study, we have processed visible near infrared (VNIR) and shortwave infrared (SWIR) bands of Advanced space-borne thermal emission and reflection radiometer (ASTER) data to detect surface mineralization signatures in Mundiyawas - Khera area in Alwar basin, north-eastern Rajasthan, India using spectral angle mapper (SAM). The potential of SAM method to detect target under variable illumination condition was used to delineate galena, chalcopyrite, malachite etc. as surface signatures of mineralization. It was ensured that the identified surface anomalies were spectrally pure using pixel purity index. Spectral anomalies were validated in the field and also using X-Ray diffraction data. Spectral anomaly maps thus derived were integrated using weight of evidence method with the lineament density, geochemical anomaly, bouger anomaly maps to identify few additional potential areas of mineralization. This study thus establishes the importance of remote sensing in mineral exploration to zero in on potentially ore rich but unexplored zones.

1. Introduction

Copper is one of the most widely used metals in India and its usage is next only to iron and aluminium in terms of volume. The Copper mineralization in Alwar District, Rajasthan, India has been recorded within the Kushalgarh, Sariska and the Thanaghazi Formations of the Ajabgarh Group (Mukhopadhyay, 2009). Presence of numerous old workings, huge mine dumps, slag heaps in the Jodhawas and Shyampura area in the Kushalgarh Formation within the biotite- marble and quartz- marble rocks and fine dissemination, stringers and small veins of mostly malachite are indications of Cu mineralization in the area (Heron, 1953; GSI, 2011, 2016). Surface indicators include malachite stain and specks of chalcopyrite within the brecciated quartzite. The Geological Survey of India (GSI) (2016) reported Cu mineralization within the Thanaghazi Formation is evidenced by the presence of malachite, chalcopyrite and bornite. Cu minerals occur as dissemination and stringers within the tremolitic marble, carbon phyllite host rocks. According to Dr S K Wadhawan, deputy director general, GSI, "A 108.10-metre-thick copper mineralization from the Alwar basin of the north Delhi fold belt found. The tentative resource of copper is about 11 million tonnes with sporadic presence of gold and silver that are 5–15 parts per million" (Times of India, 2012). GSI further reported that this is the first report of such large deposit from Alwar Basin and might turn out to be the largest occurrence in Western India.

Conventional mapping and exploration techniques may not be adequate in difficult and inaccessible terrains. Hence, there is a need to use modern techniques such as remote sensing to overcome this limitation and identify potential deposits of copper (Yang et al., 2005). Intensive field exploration activities are required in mineral exploration for understanding the geology of the area through lithological and mineral mapping, so that it leads to potential exploration targets (Sabins, 1999a; Sun et al., 2001; Thompson et al., 1999). For this purpose, remote sensing is already a validated tool for mapping indicator minerals of alteration and mineralization zones (Asadzadeh and de Souza, 2016; Kruse, 1996, 2012, Kruse et al., 2003; Ramakrishnan et al., 2013; Ramadan and Kontny, 2004). Traditionally, geological mapping and mineral exploration methods utilize physical characteristics of rocks and soils such as mineralogy, weathering characteristics,

* Corresponding author.
E-mail address: shovan.iitb@gmail.com (S.L. Chattoraj).

https://doi.org/10.1016/j.jag.2020.102162
Received 26 February 2020; Received in revised form 24 April 2020; Accepted 15 May 2020
Available online 28 May 2020
0303-2434/ © 2020 The Authors. Published by Elsevier B.V. This is an open access article under the CC BY license (http://creativecommons.org/licenses/BY/4.0/).

geochemical signatures, and landforms to determine the nature and distribution of geologic units and to determine exploration targets for economic minerals (Bishop et al., 2011; Goetz et al., 1985, 2001, 2009). But remote sensing can detect subtle mineralogical differences, often important for distinguishing background rock formations and potential mineralization zones, which are often difficult to map during field survey (Boardman and Kruse, 1994; van der Meer et al., 2001; van der Meer et al., 2012; van der Meer, 1999, 2012, Madani et al., 2003). However, demarcating the mineral prospects zones using space-borne data is still in developing stage in India. Rajasthan state is rich in economical mineral deposits which need to be further explored and extended. Demonstration of remote sensing technology with reference to the quantitative information of the mineral constituents can further fill the gap between remote sensing and geochemistry (Borengasser et al., 2007; Cloutis, 1996; Chattoraj et al., 2018; Jain and Sharma, 2019; Kumar et al., 2020; Sengar et al., 2020). The aim of the study is to demonstrate the applicability of image processing techniques and spectral analysis of multispectral imagery in locating and characterizing potential copper rich zones in parts of Alwar District, Rajasthan, India.

2. Study area and geological setting

The area of Investigation, Mundiyawas-Khera is located 5 km southwest of Thanagazi Tehsil Head Qaurter, Alwar District, Rajasthan. Geographically Mundiyawas-Khera area covers the longitudes 76̊ 12′00″E to 76̊ 23′00″E and latitudes 27̊ 26′45″ N to 27̊ 26′00″N. The study area covers parts of Alwar district of which the research focusses more on Khera block. It forms a part of the Alwar basin of North Delhi Fold Belt comprising rocks belonging to the Thanagazi Formation of the Ajabgarh Group of the Delhi Supergroup (Sinha-Roy et al., 1998; Gupta et al., 1981). Ridges of rocky and precipitous hills are observable features in the region. Geologically the area consists of Pre-Cambrian rock units belonging to Aravalli and Delhi Super Group (Fig. 1).

A thick pile of Proterozoic metasedimentary and metavolcanic sequences belonging to the Delhi Supergroup are exposed in the area (Chowdhury et al., 1984). These metasediments overlie basement gneisses with an unconformity (Naha and Mohanty, 1988). The study area exposes rocks of the Delhi Supergroup (DSG), which are classified into the Raialo Group, the Alwar Group and the Ajabgarh Group. The Raialo Group unconformably overlies gneisses of the basement, which contains rafts of quartzite and enclaves of amphibolite. The Raialo Group includes a thick lower sequence of vitreous white quartzite of Serrate Formation, which is overlain by a thick volcano-sedimentary sequence (Tehla Formation) constituting the upper part of Raialo Group. A well-developed unconformity represented by polymictic conglomerate and a structural break constrains the interface of Raialo and Alwar Group of rocks. The rocks of the Alwar Group have been classified into the Rajgarh, Kankwarhi and Pratapgarh Formation. The generalized sequence of the Alwar Group is a basal conglomerate, arkose and quartzite followed by a sequence of argillaceous and impure calcareous rocks represented by pelitic schist containing different mineral assemblages, impure marble and para-amphibolite, which in turn is followed by a sequence of mainly arenaceous rocks with some amount of pelitic sediments. The Ajabgarh Group of rocks conformably overlies the predominantly quartzitic Alwar Group of rocks. It comprises metamorphosed argillites with intercalated arenites and subordinate carbonates. The Ajabgarh Group is subdivided into three Formations. The lower unit is mainly a carbonate facies (Kushalgarh Formation) and is succeeded by ferruginous quartzite-phyllite-quartzite sequence (Sariska Formation). The upper Thanagazi formation is composed of carbon phyllites (often tuffaceous), andalusite-biotite-sericite-garnet-chlorite schist and some doubtful felsic volcanic rocks. Later intrusives mainly include metabasic rocks and granites.

Western Region, GSI upon subsurface drilling operation in the area

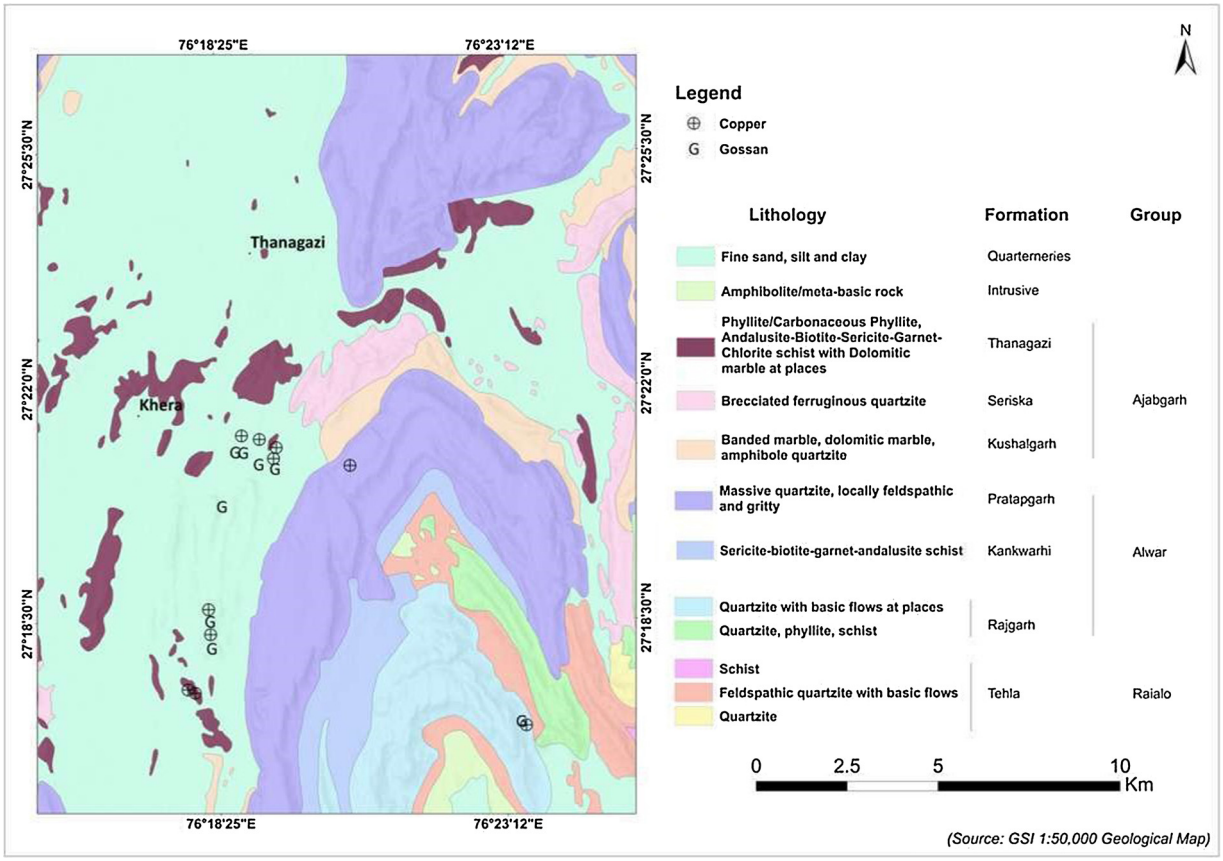

Fig. 1. Lithological Map of the study area with generalized stratigraphy (after Roy and Purohit, 2015; GSI, 2016).

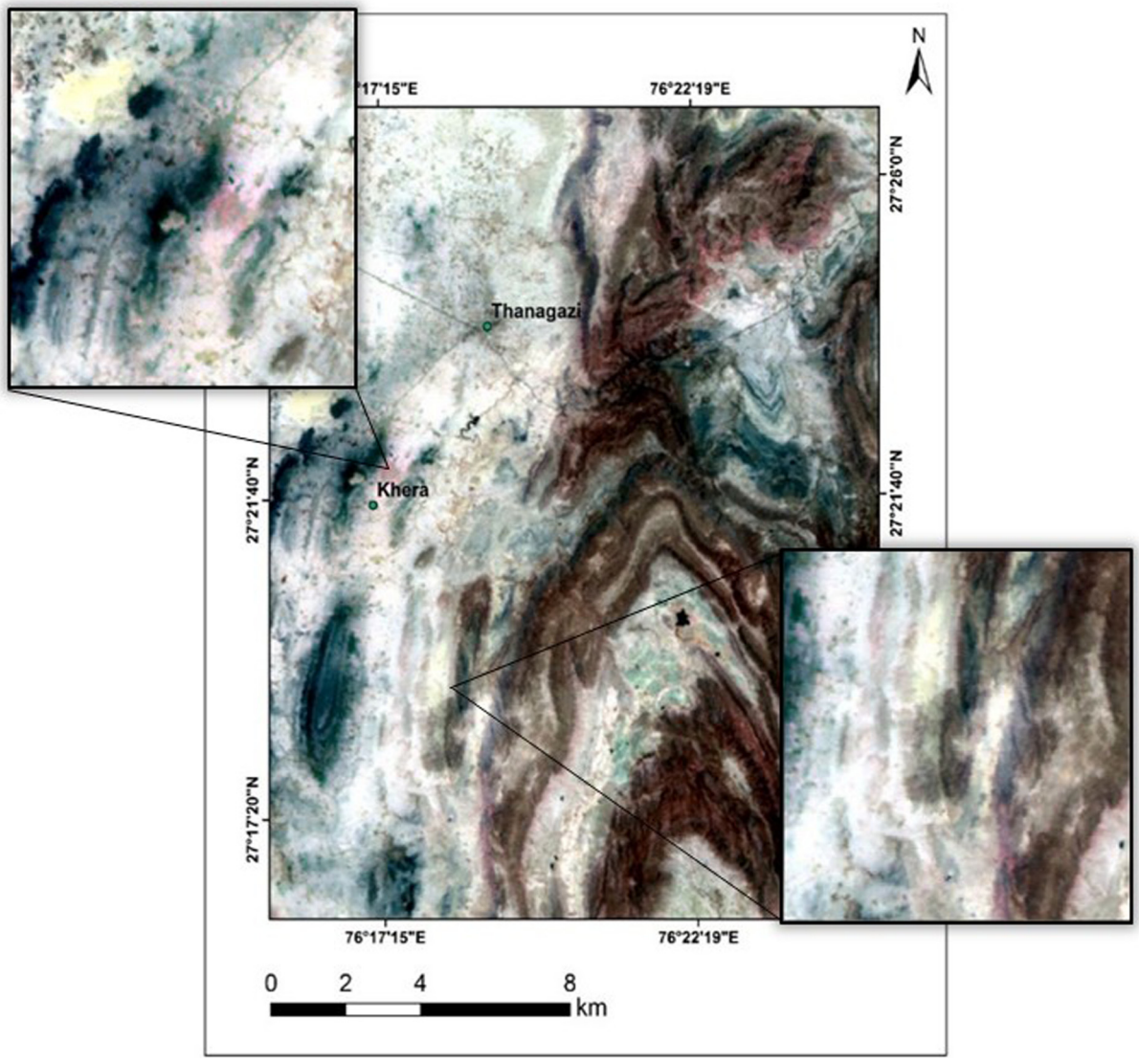

Fig. 2. False Colour Composite Image of ASTER (R: G: B = 4:6:8).

has reported more than 100 m thick sulphide mineralization associated with the meta volcano-sedimentary sequence (Khan et al., 2013). The ore mineralization mainly consist of chalcopyrite, arsenopyrite and pyrrhotite. The mode of occurrence is mostly in the form of disseminations, veins, stringers and foliation parallel layers which at times show discordant relationship (Khan et al., 2014). As far as the felsic volcanic host is concerned, ore mineralization occurs in dissemination form, at places as segregate in association with biotite which mostly occurs as rhombic, rectangular in stretched shape (Khan et al., 2013, 2014). This is indicative of syngenetic-type copper mineralization within the felsic volcanics as happened in case of Khetri copper deposit also (Golani et al., 1992, Banerjee, 1980; Pant et al., 2015; Khan and Sahoo, 2012). Hence, it is widely felt that the felsic volcanism is one of major force behind emanation of the mineralization, which got concentrated along the foliation planes, axial planar cleavages and other weak planes developed during late phase deformation. However, hydrothermal activity in the area must be prevalent phenomenon as evidenced by presence of quartz-carbonate veins within the felsic and dolomitic marble host rocks. Late phase silica metasomatism is quite prominent as manifested by development of tremolite within the dolomitic marble at metasomatic contact zones. A reducing depositional condition for sulphide mineralization is favoured by the occurrences of carbon phyllite layers and carbonate veins (Boopathi, 2010). Khan et al., 2012 and 2013 reported that widespread distribution and association of sulphide minerals (dominated by chalcopyrite, pyrrhotite and arsenopyrite) within the meta-greywacke, quartzite, felsic volcanics and their altered varieties in different modes suggest a volcanic origin for copper mineralization. It has been recommended that adjoining areas can be further explored using the mineralization controls.

3. Materials and methods

3.1. Pre-processing

ASTER L1B data is used for mineral mapping and spectroscopic analyses in this study. Pre-processing is carried out prior to mineral mapping. A specific radiometric artefact associated with ASTER data is 'crosstalk' effect, caused by signal leakage from band 4 into adjacent bands 5 and 9 (Kalinowski and Oliver, 2004). Although the impact of crosstalk is negligible during image analysis, crosstalk correction has been applied prior to any further processing because the margin of error caused by crosstalk may have more considerable effect on the assumed data analysis than the degradation of image quality. Following crosstalk correction, radiometric and atmospheric corrections have been done. Atmospheric correction done using IARR (Internal Average Relative Reflectance) method gave out satisfactory reflectance images. As this

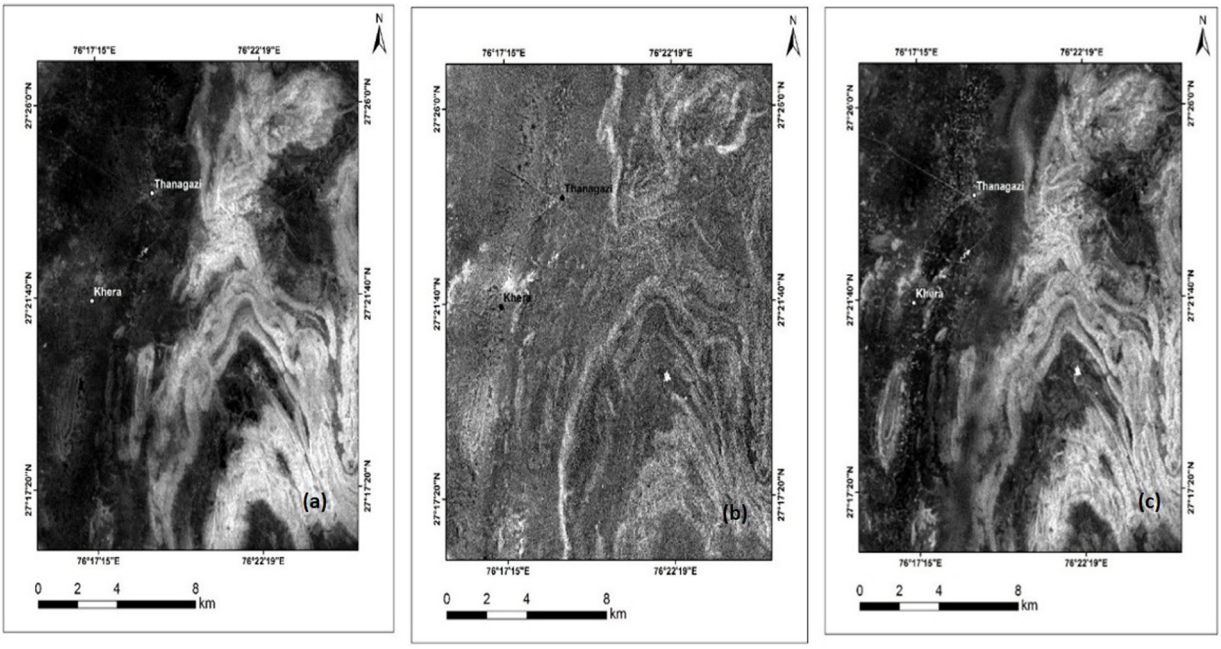

Fig. 3. Band Ratios indicating (a) Alunite/Kaolinite (4/6) (b) Sericite (5/6) (c) Epidote (5/8).

work takes substantial cues from data integration from multiple sources, as satellite data i.e. ASTER L1B, Resourcesat -1 LISS IV and Landsat 8 OLI data, the Bouguer gravity anomaly map of the World Gravity Map (WGM2012), georeferenced geochemical data points from GSI, 2016 report was projected onto WGS 84 datum and UTM Zone 43 Co-ordinate system during the pre-processing stage for the mentioned study area. Integration of all thematic layers including the interpolation was carried out at the same scale with same confirmed ground-based geo-locations for compliance of all layers to maintain synergy.

3.2. False colour composite (FCC) and band ratios

Just like vegetation is enhanced in a standard FCC due to high reflectance in the NIR region, Altered zones can also be visually enhanced by applying suitable band combinations. The SWIR false colour image created by applying bands 4, 6, and 8 to the channels, Red, Green and Blue respectively is useful for identification of alteration (Fig. 2) (Yajima et al., 2007). This is due to the fact that major altered minerals have characteristic spectral features in the SWIR region.

Intending to derive more information from the imagery, band ratios that highlight specific altered minerals have been generated. The characteristic absorption dips of altered minerals help to generate mineral specific band ratios. The ratios 4/6, 5/6 and 5/8 indicate the minerals Alunite/Kaolinite(Argillic), Sericite (Phyllic) and Epidote (Propylitic) respectively because of absorption dips at bands 6 and 8 (Fig. 3) (Yajima et al., 2007).

Moreover, Argillic alteration, phyllic alteration, propylitic alteration including calcite can be identified by the color composite image of band ratios by applying argillic alteration to red, phyllic alteration to green and propylitic alteration to blue channels. By doing so, the alteration assemblage can be visualized from the resultant color composite (Fig. 4) (Table 1).

3.3. Mineral mapping

MNF (Minimum Noise Fraction) is applied on the pre-processed image to reduce the dimensionality followed by PPI (Pixel Purity Index) to find the spectrally pure pixels. The reflectance spectra of the most spectrally pure pixels are matched with a reference spectral library to identify the mineral. Higher scores on a scale of 0–1 mean best matches. Considering this criterion and also the user's knowledge about the area and pattern of mineral occurrences, the spectra with best match is chosen as a mineral endmember. The endmembers are then used to perform classification ideally on the inverse MNF image. In this study, Mineral mapping has been done using SAM (Spectral Angle Mapping) classification technique (Fig. 5, Table 2).

In SAM classification, the spectral similarity between the image spectra and the reference spectra is calculated. The spectral similarity is measured by calculating the angle between the two spectra, treating them as vectors in n-dimensional space (Rowan and Mars, 2003). The reference spectra in this case was extracted from the image after matching it with both library as well as laboratory generated spectra. Smaller angles between the two spectra indicate high similarity and high angles indicate low similarity. The spectral threshold value by default is 0.1. This threshold value for each endmember was reduced gradually until the classified pixels coincided with the lithology of the area.

3.4. Lineaments and lineament density

Lineaments extracted from ResourceSat-1 high resolution linear imaging self-scanner (LISS-IV) and Landsat-8 Operational Land Imager (OLI) satellite imagery (Roy et al., 2014; Ganduri et al., 2018; http://www.eotec.com/images/IRS_-_Current_and_Future). Major structural features in the study area were extracted using directional filtering technique (Chavez and Bauer, 1982; Pour and Hashim, 2015) (Fig. 6(a)). The lineaments mapped are of structural and geomorphological origin. The lineament density map which shows the length of lineaments per unit area is also generated (Fig. 6(b)). The corresponding rose diagram indicates that the overall strike direction of the lineaments falls in between NNW and NNE directions.

3.5. Gravity data

Bouger gravity data used in this study are point data extracted from WGM2012 Earth gravity model (2′ x 2′ resolution) provided by International Gravimetric Bureau (BGI). WGM2012 gravity anomalies are derived from the available Earth global gravity models EGM2008 and DTU10 and include 1′x1′ resolution terrain corrections derived from ETOPO1 model that consider the contribution of most surface

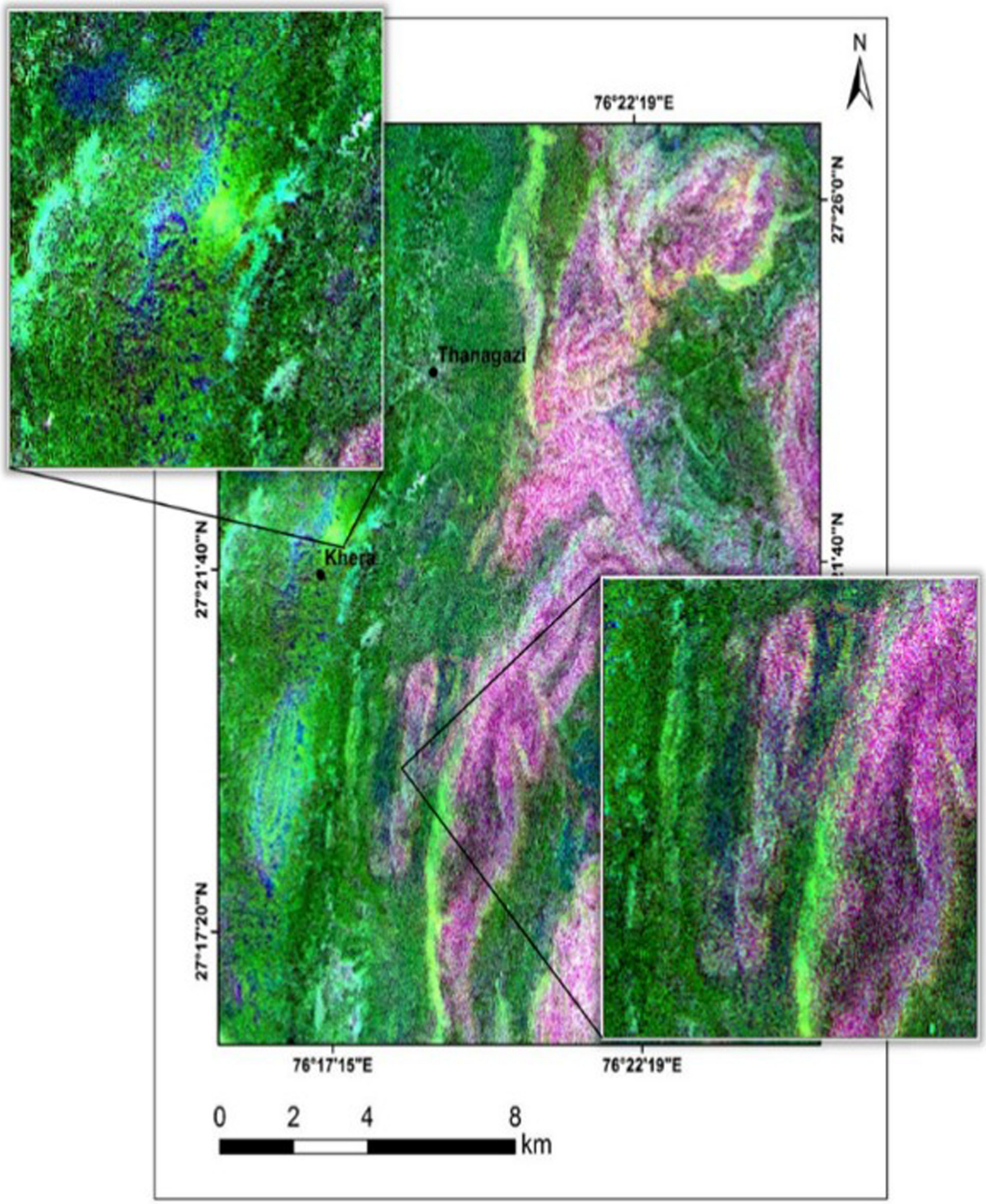

Fig. 4. Band Ratio Colour Composite.

masses such as atmosphere, land, oceans, inland seas, lakes, ice caps and ice shelves. These products have been computed by means of a spherical harmonic approach using theoretical developments carried out to achieve accurate computations at global scale. The point data containing bouger gravity values are then interpolated using spline technique to generate an interpolated raster layer (Fig. 7).

The interpolated bouger gravity map shows gravity values ranging from 57.11–97.30 mgals. Rock types within an area often contrast enough in density to cause gravity anomalies. For example, sedimentary rocks and their weathered derivatives that fill basins almost always have low densities due to dominance of Quartzo-feldspathic minerals and are characterized by gravity lows on anomaly maps. Mafic / basic rocks, which contain high density Fe-Mg minerals are often associated with gravity highs. These differences can be used to map large regions where rocks are inaccessible or concealed, to look for faults responsible for juxtaposing rocks of different densities or to infer structures such as basins, arches and buried intrusions.

Table 1
The evidence layers used for weighted sum overlay.

Evidence Layers	Weights Assigned (On a scale of 1–5)
Cu concentration map	2
Mn concentration map	1
Ti concentration map	1
Bouger Gravity Map	1
Lineament Density Map	3
Pyrite mineral map	4
Malachite mineral map	4
Chalcopyrite mineral map	5
Galena mineral map	4

3.6. Geochemical sampling

Geochemical data for the study area was collected from GSI report (2016). As per the report, the sampling was done from lower order streams. The samples were analyzed by XRF (X-ray fluorescence) and ICPMS (Inductively Coupled Plasma Mass Spectrometry) methods. The elements of interest from this geochemical analysis are Mn, Ti and Cu. However, Mn and Ti are available as MnO and TiO_2 respectively from which proportions of Mn and Ti are extracted by oxide to element conversion. The extracted weight percentages are interpolated using spline method to generate individual concentration maps for Mn, Ti and Cu (Fig. 8). Spatial distribution of other important elements was also plotted using IDW interpolation method (Fig. 9). Lack of Mn and Ti can be seen near Khera area (Fig. 8). Likewise, an anomalous presence of copper can be observed near Khera where Mn and Ti concentrations are also less or absent (Fig. 8).

3.7. Weighted sum overlay

The Weighted Sum function overlays several rasters, multiplying each by their given weight and summing them together. In this study, the layers used for overlay are Lineament Density, Gravity, Geochemical maps (only Mn, Ti and Cu) and mineral map produced using SAM method. Prior to overlay, all the layers are standardized to a common range (1–10) so as to avoid any discrimination in assigning weightages. Out of these layers, maximum weightage is given to mineral map followed by geochemical maps, lineament density and gravity. The output of the weighted sum overlay will be a favourability map for potential copper deposits in the study area (Fig. 10).

The weights assigned for the corresponding evidence layers for use in the Weighted Sum Overlay technique is shown in the table below. Based on the weights assigned to each layer, their importance will be reflected in the Overlay analysis. The weights are assigned to the layers on the basis of their relevance and reliability to the present study. For instance, the graviy layer used is of a coarser resolution (2′ x 2′) and is more apt for small scale studies. Hence, the least weightage is assigned for this layer. The interpolated geochemical concentration maps (Cu, Mn, Ti) are also assigned lesser weightages as the sampling was done at 2 km interval. The mineral maps are given higher weightages because in these layers, each pixel (15 m) is classified based on their spectral properties, which makes it more reliable than the others.

Table 2
Number pixels and area covered ((m^2) by of the each end member class.

Sl. No	End member Mineral	Pixel count	Area (m^2)
1	Galena	19	4275
2	Chalcopyrite	1094	246,150
3	Malachite	346	77,850
4	Andalusite	3934	885,150
5	Pyrite	204	45,900

4. Results and discussion

ASTER has prodigally been used for mapping and detection of Cu-

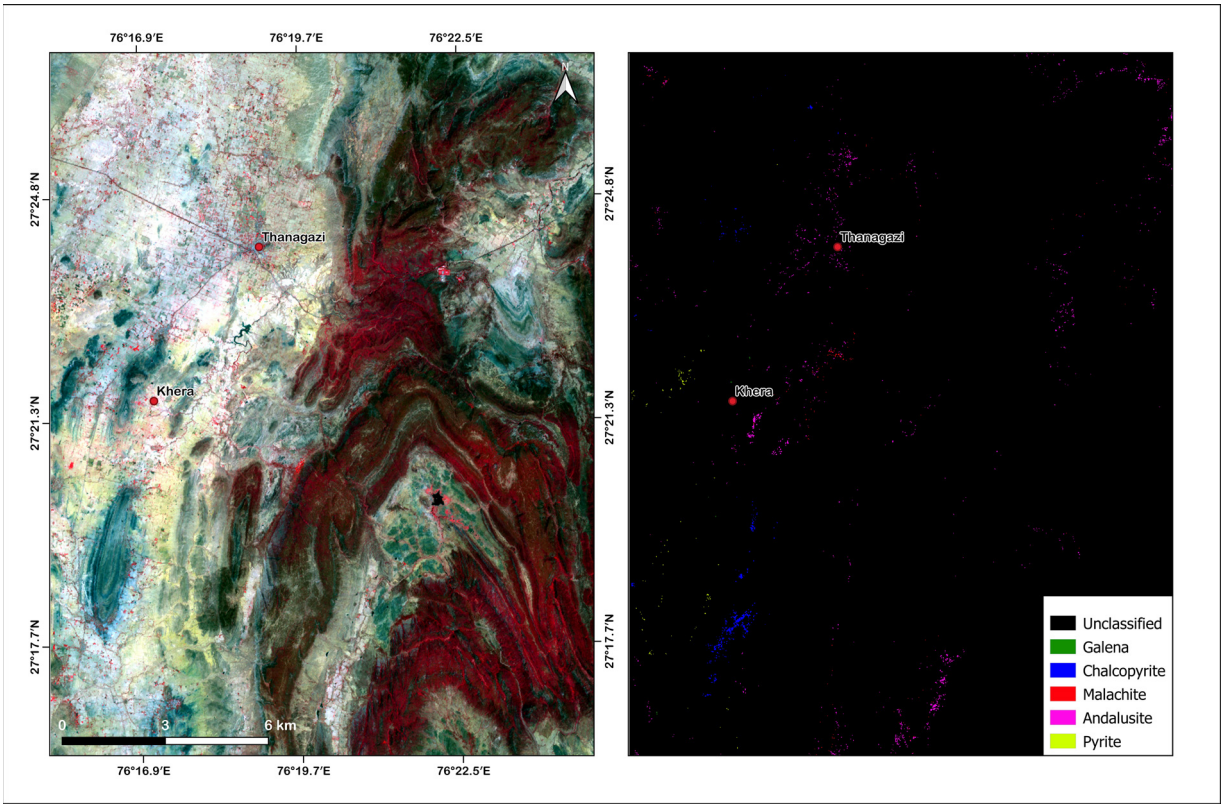

Fig. 5. SAM classified Mineral Map.

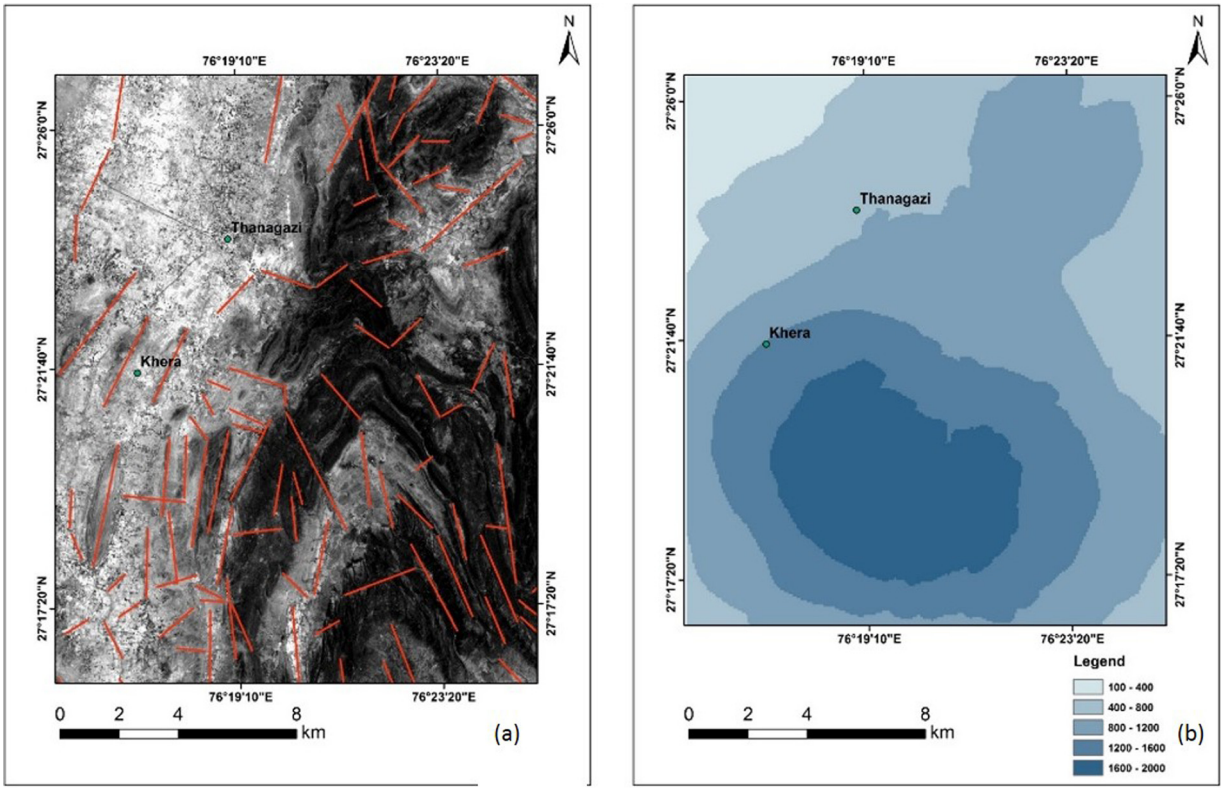

Fig. 6. (a) Lineament and (b) Lineament density map.

mineralization (Alimohammadi et al., 2015; Amer et al., 2010; Chen et al., 2010; Gad and Kusky, 2007; Gomez et al., 2005; Guha et al., 2019; Pour and Hashim, 2011, 2012a, 2012b; Rowan et al., 2003; Rowan and Mars, 2003). SAM has widely been used in spectral remote sensing to map the surface expressions in all application fields (Van der Meer and Jong, 2003; Kodikara et al., 2015). SAM does not address the problem of spectral mixing (Pour and Hashim, 2014; Sanjeevi and Abhishekh, 2006; Sanjeevi, 2008). The most erroneous assumption made with SAM is that the endmembers chosen to classify the image represent the pure spectra of the reference material (Girouard et al., 2004; Kalinowski and Oliver, 2004; Kodikara et al., 2015; Pour et al., 2017; Rao and Guha, 2018; Zhang and Li, 2014). The reference spectrum in this case belongs to a pixel that comprises spectra of several other materials including the mineral of interest. So, the pixels classified on the basis of this reference spectra may not entirely consist of a particular mineral but it will also contain the mineral that is being looked for, because the minerals present within that pixel have similar chemical composition and belong to the same parent mineral group. Hence, the mineral map seems to be unaffected by this problem.

The accuracy of a mineral map can be determined by the degree of coincidence it has with the corresponding lithology, and also with band ratios and FCC (Hewson et al., 2005; Ninomiya, 2004). Point to point ground validation of the classified mineral map revealed a substantial match at the scale under consideration. To further strengthen this, XRD (X-ray diffraction) analysis of representative samples validates the purity of the image spectra of mineral end-members. For example, the presence of malachite was verified in the field (Fig. 11(a)). The lab generated spectra of the sample collected from the field shows three prominent absorption dips at 1.4, 1.9 and 2.2 μm (Fig. 11(b)). The laboratory spectrum of malachite was compared with the ASTER reflectance spectrum from the same location from where the sample was collected. Both the spectra almost match with each other and a prominent absorption dip around 2.2 μm was observed in common between the two spectra (Fig. 11(c)). Infrared spectra of malachite up to 14 μm also help characterization of malachite Fig. 11(d). The XRD results of the sample collected from the field also helps to further validate the presence of malachite, based on the characteristic peaks of the XRD plot (Fig. 11(e)).

It is observed from the lineament map that comparatively more number of linear structural features are present towards south-east of Khera area which may indicate possible zone of structural weakness. From the lineament density map it is also observed that the density is more towards the south-east direction of Khera. High lineament density values can be correlated with alteration zones to a certain extent coupled with possible structural weakness due to the presence of fractures / faults etc. which may have acted as conduits for emanation of hydrothermal fluids. However, the actual relevance of lineament density to copper deposits can be known only after the overlay process i.e., integration with other geophysical parameters.

The area of interest i.e., Khera and surroundings is mostly associated with almost high gravity values. One more noteworthy observation is that, of all gravity values (57.11–97.30 mgals) of the study area, the known locations of copper and gossan occurrences fall within a range of 74.88–80.20 mgals. The exact reason for this cannot be accurately inferred since the gravity data available is only for a regional level. However, it is inferred from the study that gravity range in indicative about high density structure in depth and hence, was taken as a thematic layer.

The distribution of elements in the surface is largely governed by the background elemental constitution, ore systems developed and secondary weathering processes. The mobile elements are mainly controlled by the process of weathering, whereas surrounding/underlying lithology is the key factor controlling immobile to slightly mobile elements (Mason and Moore, 1985). Taking these facts into consideration, a general interpretation, has been arrived at, to target potential copper occurrences / deposits. ÖZGÜR, 1993 reported selective absence of Mn and Ti among common minor and trace elements indicating blind copper deposits. Therefore, absence of Mn-Ti minerals should be considered as a favourable criteria for copper occurrence. The geochemical concentration maps for the elements Mn, Ti and Cu prepared on this

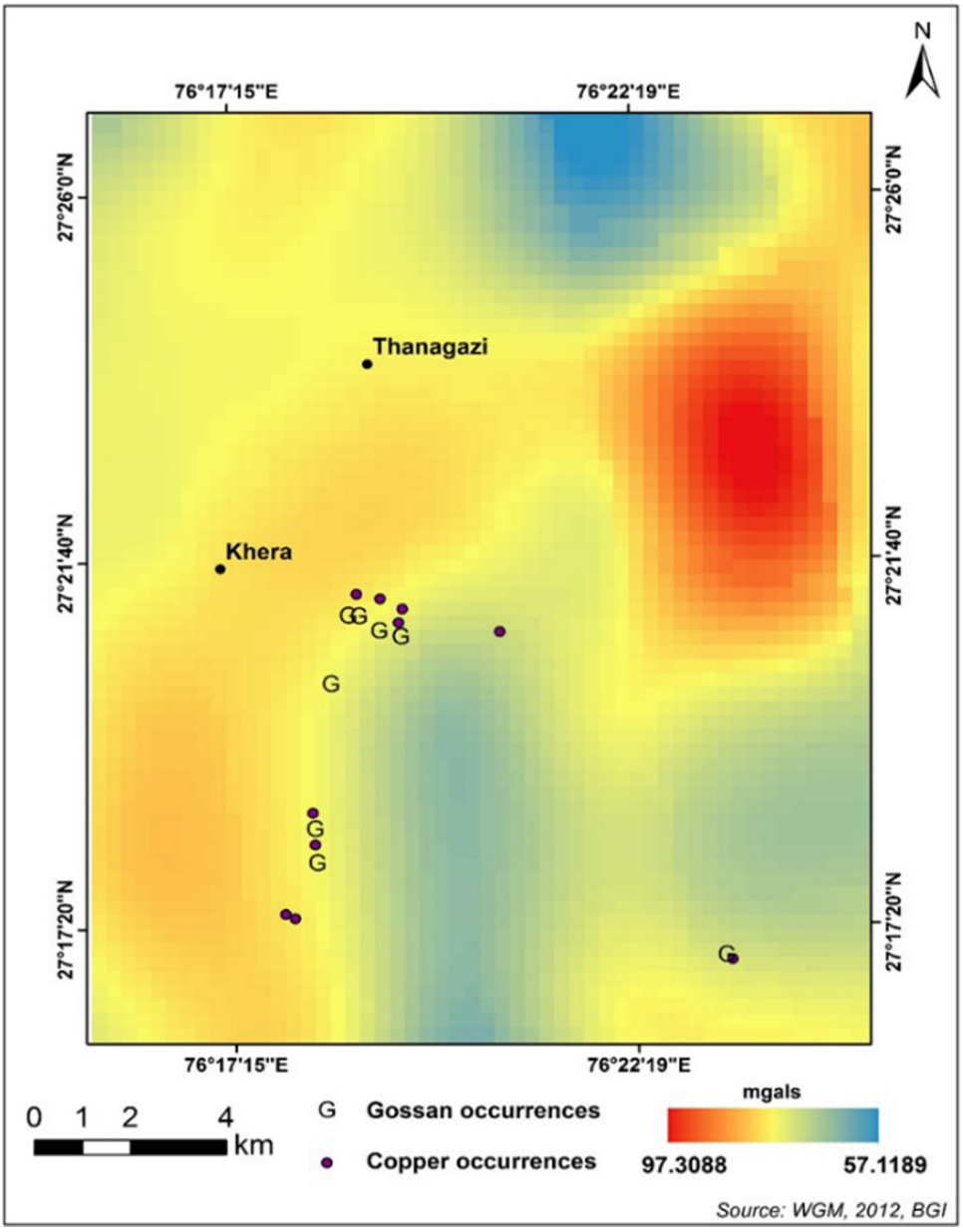

Fig. 7. Gravity Anomaly map overlaid with known Copper and Gossan locations.

basis give satisfactory results. As expected, absence of both Mn & Ti can be seen near Khera area (Fig. 8(a),(b)). Also, an anomalous presence of copper can be observed in this area where Mn & Ti concentrations are also less or absent (Fig. 8(c)). This finding correlates with the surface indications in the form of malachite staining observed during field work. Notably, malachite is a prominent pathfinder for copper.

The area is dominated by base metal mineralization and hence, altered minerals and pathfinder elements/ minerals (e.g. Cu-indicators like chalcopyrite, malachite and sulphide rich phases like pyrite and galena) play an important role, if the ore mineralization is to be addressed based on surface indicators (Banerjee, 1980; Boopathi, 2010; Golani and Narayan, 1992; Khan and Sahoo, 2012, Khan et al., 2013, 2014, Mendas and Delali, 2012; Mukhopadhyay, 2009; Nigam and Geological Survey of India, 2016; Pant et al., 2015; Sengar et al., 2020). This is why the SAM classified outputs has been given maximum weights, immediately followed by prevalent surface geochemical signatures, lineament density and gravity. It is also noted that lineament map and gravity maps are swapped there happens no significant to final weighted overlay.

The resultant of the weighted sum overlay visually infers that favourable areas for copper occurrences / deposits predominantly lie between east and south of Khera. The result concurs with all the evidence thematic layers. Apart from the favourable areas in the central region of the study area, some potential areas can be seen towards the south of Khera. Pixels classified as chalcopyrite in the mineral map as well as FCC highlighting alteration almost coincide with the same area which gives a strong clue of copper occurrence / deposit in the area (Figs. 4 and 5).

5. Conclusions

Chalcopyrite is the primary ore mineral of copper in the study area. SAM output shows the presence of chalcopyrite towards the south-east of khera. In the copper concentration map derived from stream sediment geochemical analysis, it can additionally be seen that there is an anomalous presence of copper in the central region of the study area. The approach used in this study helps to localise the area for further exploration with the help of Earth Observation & Ancillary data. In this

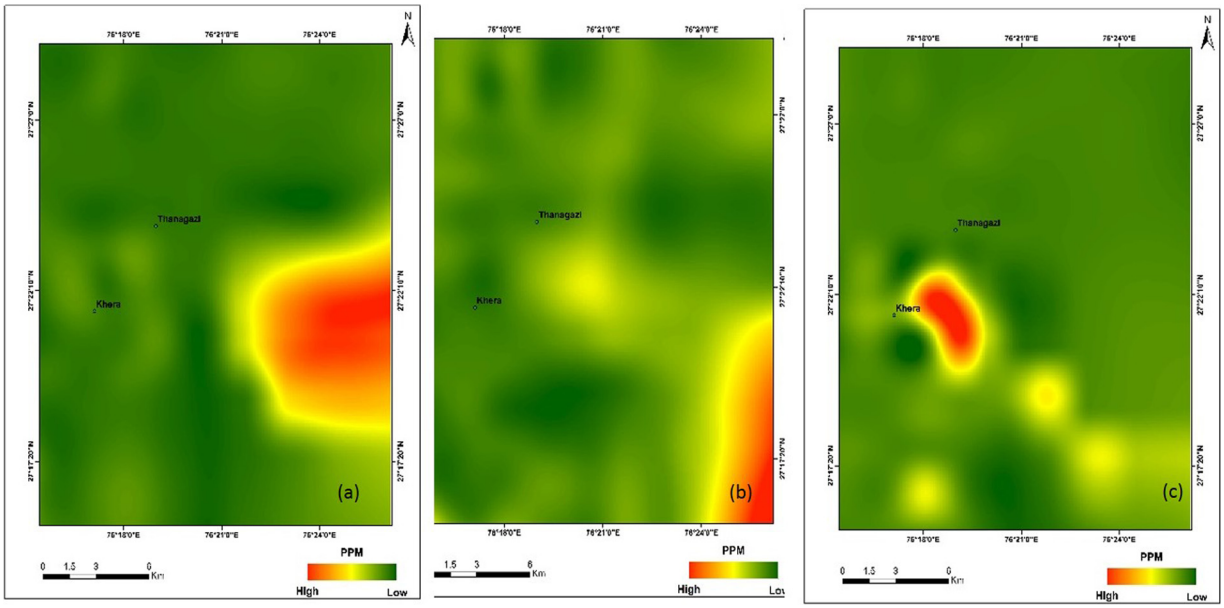

Fig. 8. Maps showing distribution of (a) Mn, (b) Ti and (c) Cu in stream sediment samples with known Copper and Gossan locations.

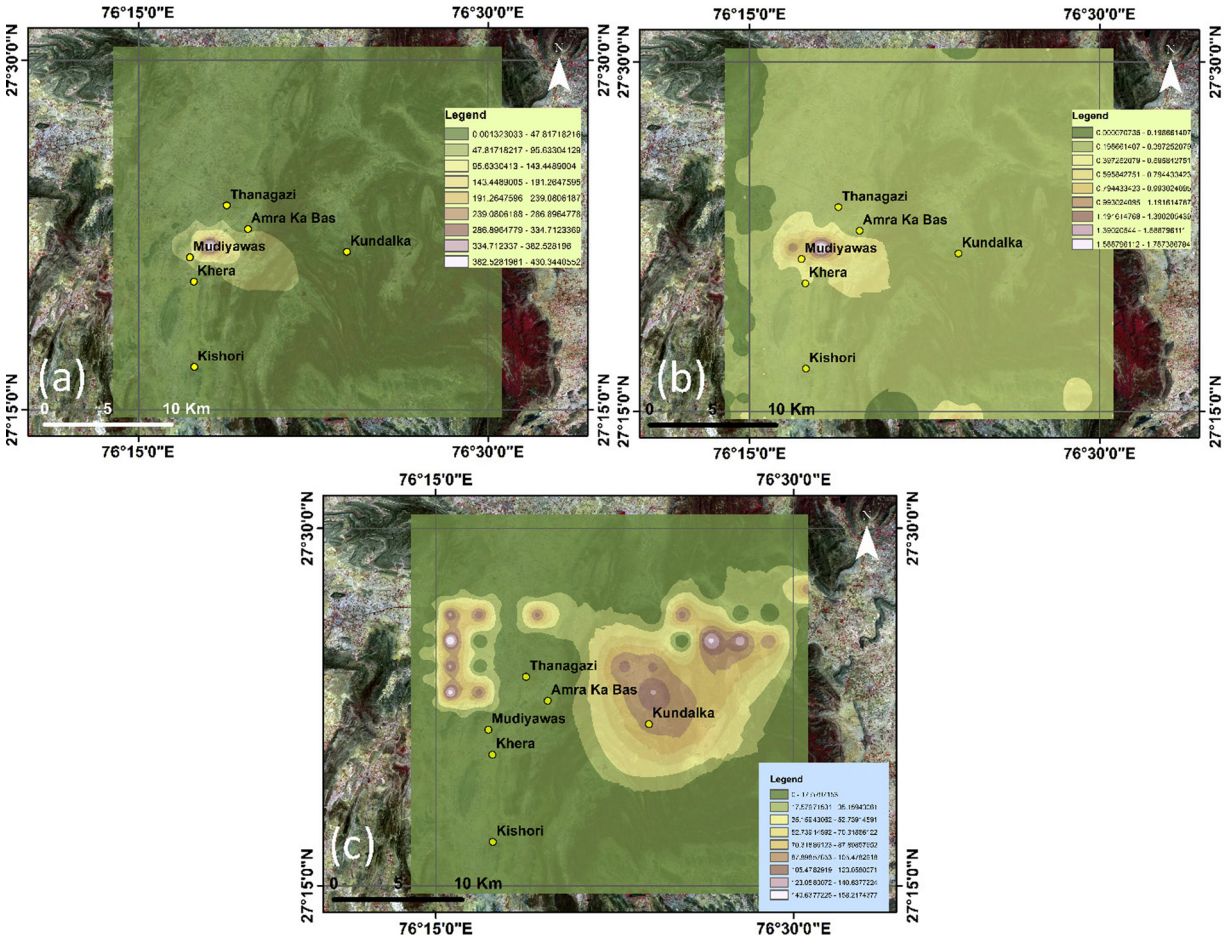

Fig. 9. Stream sediment concentration maps of (a) As, (b) Bi and (c) Cd.

case, even though there are surface indications of copper like malachite near Khera area, relatively unexplored areas towards the south of Khera should also be explored intensively as they seem to be promising for potential copper deposits.

This study also gives an insight into the exploration strategy. Prior to mineral mapping or any spectroscopic studies, a suitability study for areas suitable for mineral mapping can be adopted. The mineral mapping of such in turn gives a final output at pixel level in terms of mineral classification.

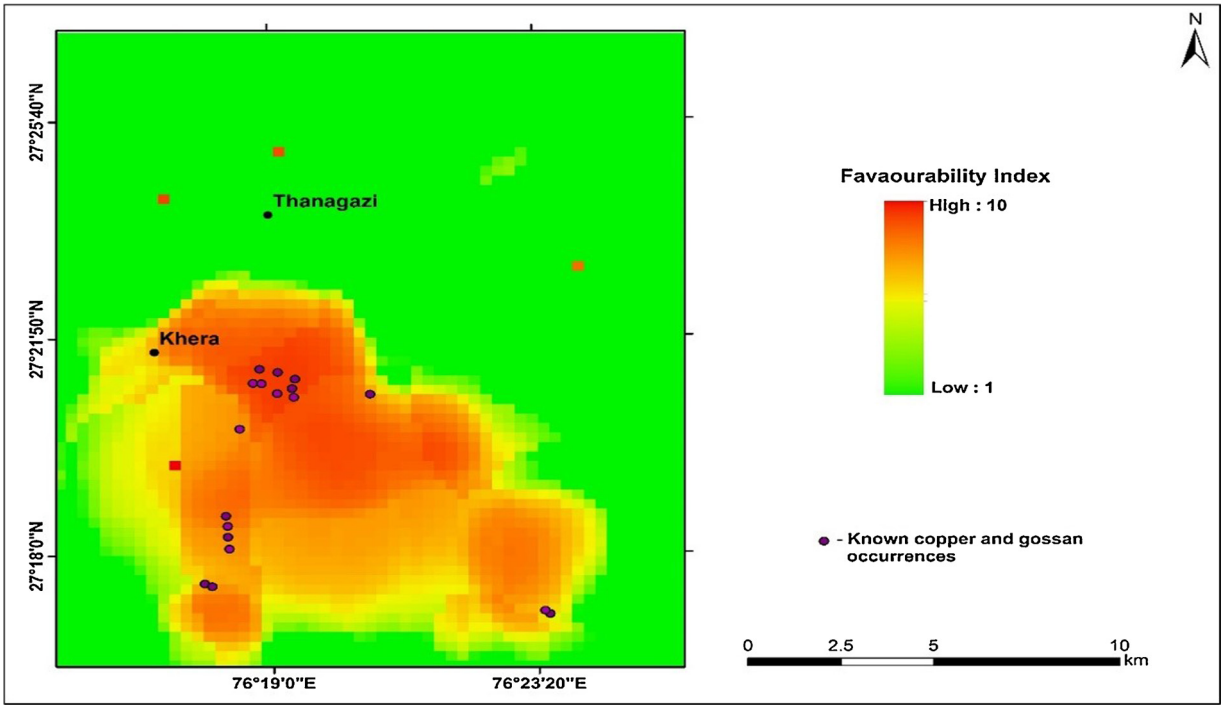

Fig. 10. Favourability Index.

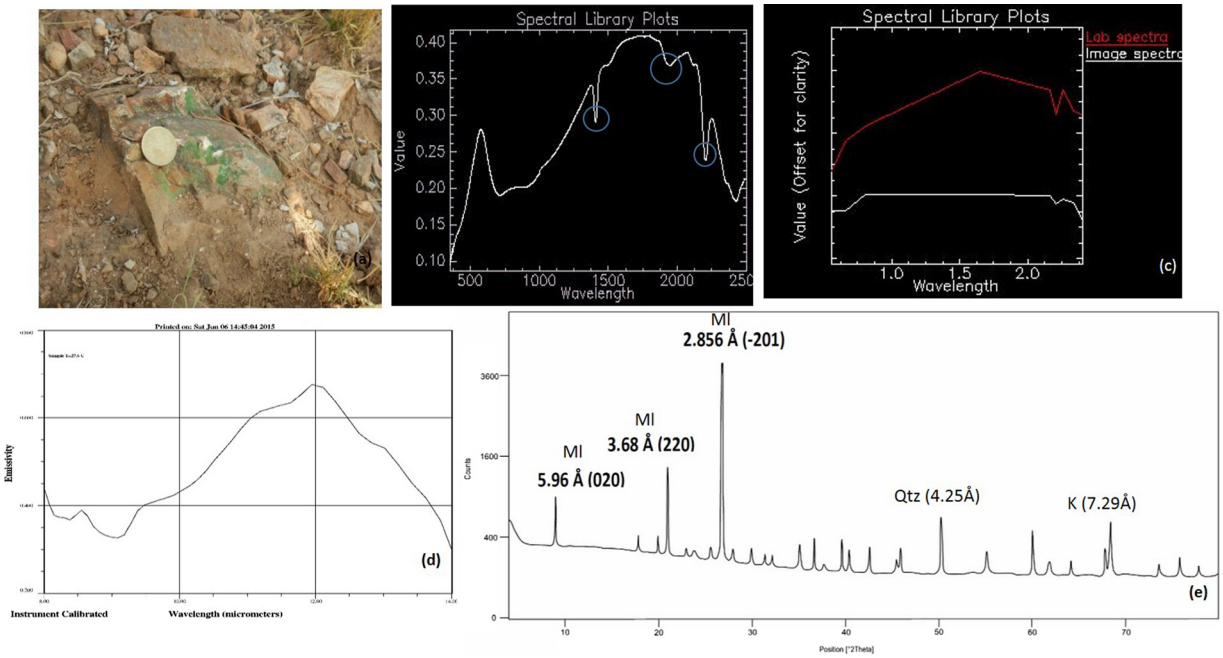

Fig. 11. (a)Malachite stains on quartzite (b) VNIR Lab spectra of malachite showing. prominent absorption dips (c) Comparison of Lab and image spectra (VNIR) (d) MIR Lab spectra of malachite showing prominent absorption dips (e) Characteristic XRD peaks of Malachite showing typical reflection faces (Ml = Malachite, K = Kaolinite, Qtz = Quartz).

Author statement

We, the authors while submitting our revised manuscript (R1) of article entitled “Integration of remote sensing, gravity and geochemical data for exploration of Cu-mineralization in Alwar basin, Rajasthan, India” for possible publication in International Journal of Applied Earth Observation and Geoinformation journal authored by Shovan Lal Chattoraj, Gokul Prasad, Richa U. Sharma, P.K. Champati ray, Freek van der Meer, Arindam Guha and Amin Beiranvand Pour outline their individual contributions to the paper using the relevant CRediT roles, as follows:

CRediT authorship contribution statement

Shovan Lal Chattoraj: Conceptualization, Funding acquisition, Investigation, Methodology, Project administration, Resources, Software, Supervision, Validation, Visualization, Writing - original draft, Writing - review & editing. **Gokul Prasad:** Conceptualization, Data curation, Formal analysis, Investigation, Methodology, Project administration, Resources, Software, Validation, Visualization, Writing

- original draft. **Richa U. Sharma:** Data curation, Formal analysis, Investigation, Project administration, Resources, Software, Supervision, Validation. **P.K. Champati ray:** Conceptualization, Funding acquisition, Project administration, Supervision. **Freek D. van der Meer:** Conceptualization, Investigation, Methodology, Software, Validation, Visualization. **Arindam Guha:** Visualization, Writing - original draft. **Amin Beiranvand Pour:** Formal analysis, Methodology, Validation, Visualization, Writing - review & editing.

Declaration of Competing Interest

The authors whose names are listed immediately below certify that they have NO affi liations with or involvement in any organization or entity with any financial interest (such as honoraria; educational grants; participation in speakers' bureaus; membership, employment, consultancies, stock ownership, or other equity interest; and expert testimony or patent-licensing arrangements), or non-financial interest (such as personal or professional relationships, affiliations, knowledge or beliefs) in the subject matter or materials discussed in this manuscript.

Acknowledgements

This paper has immensely benefited from contributions and consultations with several students of Indian Institute of Remote Sensing and our project collaborator i.e. GSI, Western Region, Jaipur. Organizational support and overall guidance provided by Dr. Prakash Chauhan Director, IIRS and Dr. A. Senthil Kumar, Former-Director, IIRS is also duly acknowledged. SLC, RU and PKC are thankful to Indian Space Research Organization, Department of Space, Government of India for the financial support provided in EOAM project.

References

Alimohammadi, Masoumeh, Alirezaei, Saeed, Kontak, Daniel J., Alimohammadi, Masoumeh, Alirezaei, Saeed, Kontak, Daniel J., 2015. Application of ASTER data for exploration of porphyry copper deposits: a case study of Daraloo–sarmeshk area, southern part of the Kerman copper belt, Iran. Ore Geol. Rev. 70, 290–304.

Amer, R., Kusky, T., Ghulam, A., 2010. Lithological mapping in the Central Eastern Desert of Egypt using ASTER data. J. Afr. Earth Sci. 56 (2–3), 75–82. https://doi.org/10.1016/j.jafrearsci.2009.06.004.

Asadzadeh, S., de Souza Filho, C.R., 2016. A review on spectral processing methods for geological remote sensing. Int. J. Appl. Earth Obs. Geoinf. 47, 69–90. https://doi.org/10.1016/j.jag.2015.12.004.

Banerjee, A.K., 1980. Geology and mineral resources of Alwar district. Rajasthan. Rec. Geol. Soc. India 110, 137.

Bishop, C.A., Liu, J.G., Mason, P.J., 2011. Hyperspectral remote sensing for mineral exploration in Pulang, Yunnan Province. China. International Journal of Remote Sensing 32 (9), 2409–2426. https://doi.org/10.1080/01431161003698336.

Boardman, J.W., Kruse, F.A., 1994. Automated spectral analysis: a geological example using AVIRIS data, north grapevine mountains, Nevada. In: Proceedings of ERIM Tenth Thematic Conference on Geologic Remote Sensing. Environmental Research Institute of Michigan, Ann Arbor, MI. pp. I-407–I-418.

Boopathi, D., 2010. Investigatin for Copper and Associated Precious Metals, Mundiwayaskhera Area, Alwar District, Rajasthan. Unpub. GSI Final Report F.s. pp. 2008–2009.

Borengasser, M., Hungate, W.S., Watkins, R., 2007. Hyperspectral Remote Sensing: Principles and Applications. Taylor and Francis, Boca Raton, Florida, pp. 119.

Chattoraj, S.L., Banerjee, S., van der Meer, F., Champati Ray, P.K., 2018. Application of visible and infrared spectroscopy for evaluation of evolved glauconite. International Journal of Applied Earth Observation 64, 301–310. https://doi.org/10.1016/j.jag.2017.02.007.

Chen, X., Warner, T.A., Campagna, D.J., 2010. Integrating visible, near-infrared and short-wave infrared hyperspectral and multispectral thermal imagery for geological mapping at Cuprite, Nevada: a rule-based system. Int. J. Remote Sens. 31 (7), 1733–1752. https://doi.org/10.1080/01431160902926616.

Chowdhury, A.K., Gopala, K., Sastry, C.A., 1984. Present status of the geochronology of the Precambrian rocks of Rajasthan. Tectonophysics 105 (1-4), 131–140.

Cloutis, E.A., 1996. Hyperspectral geological remote sensing: evaluation of analytical techniques. Int. Jour. Remote Sensing 17, 2215–2242.

Gad, S., Kusky, T., 2007. ASTER spectral ratioing for lithological mapping in the Arabian–Nubian shield, the Neoproterozoic Wadi Kid area, Sinai. Egypt. Gondwana Research 11 (3), 326–335. https://doi.org/10.1016/j.gr.2006.02.010.

Ganduri, B., Laxmi, U., Vidyasagarachary, G.D., 2018. IRS P6-LISS IV Satellite Image Analysis For Mapping Geomorphology And Hydrogeological Features Along The Musi River From Hyderabad To Valigonda, Telangana State, India. International Journal of Engineering Science Invention 7 (8), 6–11.

Geological Survey of India, Govt. of India, 2011. Geology and Mineral Resources of Rajasthan (3rd Edition). Miscellaneous Publication, GSI: Kolkata, pp. 130 30 (12).

Girouard, G., Bannari, A., El Harti, A., Desrochers, A., 2004. Validated Spectral Angle Mapper Algorithm for Geological Mapping: Comparative Study Between Quickbird and Landsat-tm, in: XXth ISPRS Congress, Geo-imagery Bridging Continents. Istanbul, Turkey.. pp. 12–23.

Goetz, A.F.H., Vane, G., Solomon, J.E., Rock, B.N., 1985. Imaging spectrometry for earth remote sensing. Science 228, 1147–1153.

Goetz, A.F.H., Chabrillat, S., Lu, Z., 2001. Field reflectance spectrometry for detection of swelling clays at construction sites. Field Anal. Chem. Technol. 5, 143–155.

Goetz, F.H.A., Curtiss, B., Shiley, D.A., 2009. Rapid gangue mineral concentration measurement over conveyors by NIR reflectance spectroscopy. Miner. Eng. 22, 490–499.

Golani, P.R., Narayan, S., 1992. Study of volcanics in Delhi Supergroup of rocks in relation to base metal metallogeny in central and southern Rajasthan and northern Gujarat. Rec. Geol. Surv. India 123, 82–88.

Gomez, C., Delacourt, C., Allemand, P., Ledru, P., Wackerle, R., 2005. Using ASTER remote sensing data set for geological mapping, in Namibia. Phys. Chem. Earth Parts A/b/c 30 (1–3), 97–108. https://doi.org/10.1016/j.pce.2004.08.042.

Guha, A., Vinod Kumar, K., Porwal, A., Rani, K., Sahoo, K.C., Aneesh Kumar, S.R., Singaraju, V., Singh, R.P., Khandelwal, M.K., Raju, P.V., Diwakar, P.G., 2019. Reflectance spectroscopy and ASTER based mapping of rock-phosphate in parts of Paleoproterozoic sequences of Aravalli group of rocks, Rajasthan. India. Ore Geology Reviews 108, 73–87. https://doi.org/10.1016/j.oregeorev.2018.02.021.

Gupta, S.N., Arora, Y.K., Mathur, R.K., Iqballuddin, B., Sahai, T.N., Sharma, S.B., 1981. Lithostratigraphic map of Aravalli Range. Records of Geological Survey of India 120, 12–26.

Heron, A.M., 1953. Geology of Central Rajasthan. Memoirs of the Geological Survey of India 79, 339.

Hewson, R.D., Cudahy, T.J., Mizuhiko, S., Ueda, K., Mauger, A.J., 2005. Seamless geological map generation using ASTER in the Broken Hill-Curnamona province of Australia. Remote Sens. Environ. 99 (1–2), 159–172. https://doi.org/10.1016/j.rse.2005.04.025.

Jain, R., Sharma, R.U., 2019. Airborne hyperspectral data for mineral mapping in Southeastern Rajasthan. India. International Journal of Applied Earth Observation and Geoinformation 81, 137–145. https://doi.org/10.1016/j.jag.2019.05.007.

Kalinowski, A., Oliver, S., 2004. ASTER mineral index processing manual. Remote Sensing Applications, Geoscience Australia 37.

Khan, I., Sahoo, P.R., 2012. . Investigation for Copper and Associated Precious Metals in KHera Block, Mundiwayas-khera Area, Alwar District, Rajasthan. Unpub. GSI Final Report F.S. GSI, pp. 2010–2012 Western Region.

Khan, I., Rai, D.K., Sahoo, P.R., 2013. A note on new find of thick copper and associated precious metal mineralisation from Alwar Basin of North Delhi Fold Belt. Rajasthan. Journal of Geological Society of India 82 495-468.

Khan, I., Sahoo, P.R., Rai, D.K., 2014. Proterozoic felsic volcanics in Alwar Basin of North Delhi Fold Belt, Rajasthan: implication for copper mineralization. Journal of Current Science 106 (1), 27–28.

Kodikara, R.L., Champati ray, P.K., Chauhan, P., Chatterjee, R.S., 2015. Spectral mapping of morphological features on the moon with MGM and SAM. Int. J. Appl. Earth Obs. Geoinf. 44, 31–41.

Kruse, F.A., 1996. Identification and mapping of minerals in drill core using hyperspectral image analysis of infrared reflectance spectra. Int. J. Remote Sens. 17 (9), 1623–1632.

Kruse, F.A., 2012. Mapping surface mineralogy using imaging spectrometry. Geomorphology 137, 41–56.

Kruse, F.A., Boardman, J.W., Huntington, J.F., 2003. Evaluation and validation of EO-1 hyperion for mineral mapping. Ieee Trans. Geosci. Remote. Sens. 41 (6), 1388–1400.

Kumar, C., Chatterjee, S., Oommen, T., Guha, A., 2020. Automated lithological mapping by integrating spectral enhancement techniques and machine learning algorithms using AVIRIS-NG hyperspectral data in Gold-bearing granite-greenstone rocks in Hutti, India. Int. J. Appl. Earth Obs. Geoinf. 86, 102006. https://doi.org/10.1016/j.jag.2019.102006.

Madani, A.A., Abdel Rahman, E.M., FA WZY, K.M., Emam, A., 2003. Mapping of the hydrothermal alteration zones at Haimur gold mine area, South Eastern Desert, Egypt, using remote sensing techniques. Egyptian Journal of Remote Sensing and Space Sciences 6, 47–60.

Mason, B., Moore, C.B., 1985. Principles of Geochemistry.

Mendas, A., Delali, A., 2012. Support system based on GIS and weighted sum method for drawing up of land suitability map for agriculture. Application to durum wheat cultivation in the area of Mleta (Algeria). Spanish Journal of Agricultural Research 10 (1), 34–43 2012.

Mukhopadhyay, S., 2009. STM of Delhi Supergroup of rocks in Jodhawas- Kushalgarh area, Alwar district, Rajasthan. Unpub. GSI Progress Report F.S. pp. 2006–2008.

Naha, K., Mohanty, S., 1988. Response of basement and cover rocks to multiple deformations: a study from the Precambrian of Rajasthan, western India. Precambrian Res. 42, 77–96.

Nigam, N.K., Geological Survey of India, 2016. Geochemical mapping of toposheet No.54 A/7 covering parts of Alwar and Jaipur districts, Rajasthan. Interim Report for the Field Season 2010-12 167 Western Region, Jaipur.

Ninomiya, Y., 2004. Lithologic mapping with multispectral ASTER TIR and SWIR data. In: Meynart, R., Neeck, S.P., Shimoda, H., Lurie, J.B., Aten, M.L. (Eds.), Sensors, Systems, and Next-Generation Satellites VII. SPIE. https://doi.org/10.1117/12.511902.

ÖZGÜR, N., 1993. Geochemical pathfınder elements of the murgul copper deposit, NE Turkey. Resource Geology Special Issue 163–168.

Pant, N.C., Kumar, S., Pandey, M., Bajaj, A.K., Kundu, A., Joshi, S., Shimyaphy, R.V.S., 2015. New insights on the genesis and controls of mineralization in khetri copper belt

and adjoining low grade Cu mineralization, north western Indian shield. In: In: Golani, P.R. (Ed.), Recent Developments in Metallogeny and Mineral Exploration in Rajasthan 101. GSI Spl. Publication, pp. 109–128.
Pour, A.B., Hashim, M., 2011. Identification of hydrothermal alteration minerals for exploring of porphyry copper deposit using ASTER data, SE Iran. J. Asian Earth Sci. 42, 1309–1323.
Pour, A.B., Hashim, M., 2012a. Identifying areas of high economic-potential copper mineralization using ASTER data in the Urumieh–Dokhtar Volcanic Belt. Iran. Advances in Space Research 49, 753–769.
Pour, A.B., Hashim, M., 2012b. The application of ASTER remote sensing data to porphyry copper and epithermal gold deposits. Ore Geol. Rev. 44, 1–9.
Pour, A.B., Hashim, M., 2014. ASTER, ALI and Hyperion sensors data for lithological mapping and ore minerals exploration. SpringerPlus 3 (1). https://doi.org/10.1186/2193-1801-3-130.
Pour, B.A., Hashim, M., 2015.). Integrating PALSAR and ASTER data for mineral deposits exploration in tropical environments: a case study from Central Belt, Peninsular Malaysia.730. Int. J. Image Data Fusion 6, 170–188.
Pour, A.B., Hashim, M., Park, Y., Hong, J.K., 2017. Mapping alteration mineral zones and lithological units in Antarctic regions using spectral bands of ASTER remote sensing data. Geocarto Int. 33 (12), 1281–1306. https://doi.org/10.1080/10106049.2017.1347207.
Ramadan, T.M., Kontny, A., 2004. Mineralogical and structural characterization of alteration zones detected by orbital remote sensing at Shalatein District, SE Desert. Egypt. Journal of African Earth Sciences 40, 89–99.
Ramakrishnan, D., Bharti, R., Singh, K.D., Nithya, M., 2013. Thermal inertia mapping and its application in mineral exploration: results from Mamandur polymetal prospect, India. J. Earth Syst. Sci. 122 (1), 93–106.
Rao, D.A., Guha, A., 2018. Potential Utility of Spectral Angle Mapper and Spectral Information Divergence Methods for mapping lower Vindhyan Rocks and Their Accuracy Assessment with Respect to Conventional Lithological Map in Jharkhand, India. J. Indian Soc. Rem. Sens. 46 (5), 737–747. https://doi.org/10.1007/s12524-017-0733-3.
Rowan, L.C., Mars, J.C., 2003. Lithologic mapping in the Mountain Pass, California area using advanced spaceborne thermal emission and reflection radiometer (ASTER) data. Remote Sens. Environ. 84 (3), 350–366. https://doi.org/10.1016/s0034-4257(02)00127-x.
Rowan, L.C., Hook, S.J., Abrams, M.J., Mars, J.C., 2003. Mapping hydrothermally altered rocks at Cuprite, Nevada, using the Advanced Spaceborne Thermal Emission and Reflection Radiometer (ASTER), a new satellite-imaging system. Econ. Geol. 98, 1019–1027.
Roy, A.B., Purohit, R., 2015. Lithostratigraphic, geochronological and depositional framework of the Precambrian basins of the Aravalli Mountains and adjoining areas, Rajasthan. India. Geological Society, London, Memoirs 43 (55-65). https://doi.org/10.1144/M43.4. 2015.
Roy, D.P., Wulder, M.A., Loveland, T.A., Woodcock, C.E., Allen, R.G., Anderson, M.C., et al., 2014. Landsat-8: science and product vision for terrestrial global change research. Remote Sens. Environ. 145, 154–172.
Sabins, F.F., 1999a. Remote sensing for mineral exploration. Ore Geol. Rev. 14, 157–183.
Sanjeevi, S., 2008. Targeting limestone and bauxite deposits in southern India by spectral unmixing of hyperspectral image data. The International Archives of the Photogrammetry. Remote Sensing and Spatial Information Sciences XXXVII (B8), 1189–1194 Beijing.
Sanjeevi, S., Abhishekh, P.V., 2006. Spectral unmixing of hyperspectral data to map bauxite deposits. Proceedings of International Society for Optics and Photonics 6405, 64051N.
Sengar, V.K., Venkatesh, A.S., Champati ray, P.K., Sahoo, P.R., Khan, I., Chattoraj, S.L., 2020. Spaceborne mapping of hydrothermal alteration zones associated with the Mundiyawas-Khera copper deposit, Rajasthan, India, using SWIR bands of ASTER: implications for exploration targeting. Ore Geol. Rev. 118, 103327. https://doi.org/10.1016/j.oregeorev.2020.103327.
Sinha-Roy, S., Malhotra, G., Mohanty, M., 1998. Geology of Rajasthan: Geological Society of India. Bangalore. .
Sun, Y., Seccombe, P.K., Yang, K., 2001. Application of IR spectroscopy to define alteration zones associated with Elura zinc–lead–silver deposit NSW Australia. J. Geochem. Explor. 73, 11–26.
Thompson, A.J.B., Hauff, P.L., Robitaille, A., 1999. Alteration mapping in exploration: application of short-wave infrared (SWIR) spectroscopy. Society of Economic Geology Newsletter 39, 16–27.
Times of India, 2012. Jaipur Edn., Copper Reservoirs With Gold Traces Found in Alwar. 2012, Feb 17. https://timesofindia.indiatimes.com/city/jaipur/Copper-reservoirs-with-gold-traces-found-in-Alwar/articleshow/11919083.cms.
van der Meer, F.D., 1999. Imaging spectrometry for geological remote sensing. Geol. En Mijnb. 77 (2), 137–151.
van der Meer, F.D., 2012. Remote sensing image analysis and geostatistics. Int. J. Remote Sens. 33, 5644–5676.
van der Meer, F.D., van der Werff, H.M.A., van Ruitenbeek, F.J.A., Hecker, C.A., Bakker, W.H., Noomen, M.F., van der Meijde, M., Carranza, E.J.M., de Smeth, J.B., Woldai, T., 2012. Multi and hyperspectral geologic remote sensing: a review. Int. J. Appl. Earth Obs. Geoinf. 14, 112–128.
Van der Meer, F.D., Jong, S.D., 2003. Spectral mapping methods: many problems, some solutions, presented at the 3rd EARSeL workshop on imaging spectroscopy. Herrsching 146–162.
Van der Meer, F., de Jong, S. (Eds.), 2001. Imaging Spectrometry: Basic Principles and Prospective Applications. Springer, the Netherlands.
Yajima, T., Yamamoto, K., Hayashi, T., 2007. Identification of hydrothermal alteration zones for exploration of porphyry copper deposits using ASTER data. Journal of the Remote Sensing Society of Japan (Japan).
Yang, K., Lian, C., Huntington, J.F., Peng, Q., Wang, Q., 2005. Infrared spectral reflectance characterization of the hydrothermal alteration at the Tuwu Cu–Au deposit Xinjiang. China. Mineralium Deposita 40, 324–336.
Zhang, X., Li, P., 2014. Lithological mapping from hyperspectral data by improved use of spectral angle mapper. Int. J. Appl. Earth Obs. Geoinf. 31, 95–109. https://doi.org/10.1016/j.jag.2014.03.007.